The paper was presented at the Tenth Meeting "New Trends in Fatigue and Fracture" (NT2F10) Metz, France, 30 August–1 September, 2010

Jena Jeong[1], Pierre Mounanga[2], Hamidréza Ramézani[3], Marwen Bouasker[3]

MULTI SCALE MODELLING BASED ON THE HYGRO-COSSERAT THEORY FOR SELF DESICCATION DEFORMATION OF CEMENT MORTARS AT EARLY AGE

MULTISKALARNO MODELIRANJE NA BAZI HIGRO-KOSERA TEORIJE ZA DEFORMACIJU U RANOJ FAZI SAMOISUŠIVANJA CEMENTNOG MALTERA

Original scientific paper
UDC: 666.971.4.019
Paper received: 31.01.2011

Author's address:
1) ESTP/IRC/LM-Lean Modeling-École Spéciale des Travaux Publics, du Bâtiment et de l'industrie (ESTP), 28 avenue du Président Wilson, 94234 Cachan cedex, France, jeong@profs.estp.fr
2) GeM, UMR CNRS 6183 - Research Institute on Civil Engineering and Mechanics, University of Nantes, Saint-Nazaire, France, pierre.mounanga@univnantes.fr
3) CRMD, UMR CNRS 6619- Research Center on Divided Materials, École Polytechnique de l'Université d'Orléans, France

Keywords
- cement based mortar
- autogenous shrinkage
- self desiccation
- multi scale approach
- hygro-Cosserat theory

Abstract

In the present paper, we concentrate on the heterogeneous cement mortars and we treat them as Cosserat-based media. The autogenous shrinkage phenomenon at early age (from 1 to 3 days after mixing) is analysed by means of the Cosserat theory. The characteristic length scale parameter L_c in this theory helps us to change the size specimen from macro-scale to micro-scale using the theoretical size effect aspects. This methodology is also capable of treating crack initiation and their appearance in the cementitious matrix, surrounding the sand-inclusions, which should occur inside the Representative Volume Elementary (RVE) of mortar subjected to self-desiccation shrinkage during hydration at early age. By taking advantage of the Nonlinear Finite Element Analysis (NFEA), numerical experiments are performed. Numerical outcomes agree well with experimental observations from Scanning Electronic Microscopy (SEM) images. It concludes that the inclusions create not only a hygro stress concentration around the grains but also the number of inclusions should influence the network in the cementitious matrix.

Ključne reči
- cementni malter
- skupljanje
- samoisušivanje
- multiskalarni pristup
- higro-Kosera teorija

Izvod

U ovom radu, pažnju smo usmerili na heterogeni cementni malter koji tretiramo kao fluid tipa Kosera. Fenomen spontanog skupljanja u ranoj fazi (od 1 do 3 dana nakon mešanja) je analiziran primenom teorije Kosera. Karakteristični parametar dužine L_c u ovoj teoriji nam pomaže u izboru dimenzija epruvete od makro nivoa ka mikro nivo primenom aspekta teorijskog dimenzijskog uticaja. Ovom metodologijom se takođe može razmatrati inicijacija prslina i njihova pojava u cementnoj matrici, u okruženju uključaka peska, a koja nastaje u Reprezentativnoj Elementarnoj Zapremini (RVE) maltera, podvrgnutom skupljanju usled samoisušivanja u ranoj fazi hidratacije. Numerički eksperimenti su izvedeni zahvaljujući prednosti analize nelinearnim konačnim elementima (NFEA). Numerički rezultati se dobro slažu sa eksperimentalnim podacima snimaka scanning elektronske mikroskopije (SEM). Zaključuje se da uključci ne izazivaju samo koncentraciju higro napona oko zrna, već i da broj uključaka takođe utiče na mrežu cementne matrice.

INTRODUCTION

In recent years, considerable interest has developed in micro-mechanical modelling of solids. This interest has been motivated by the fact that many materials have heterogeneous microstructures that play an essential role in determining their macro-scale behaviour. The response of heterogeneous solids as soil and concrete shows strong dependence on the micro-mechanical interactions between the different material phases. The classical theories of continuum mechanics have limited ability to predict such behaviours. In the current study, we take advantage of the Cosserat theory and we apply it to heterogeneous materials.

The Cosserat or so-called micropolar theory was initiated by Cosserat's brothers in 1909, /1, 2/, and it has been followed and developed /3-7/ later in the early sixties. One of the most outstanding features of this theory is that one can involve the size effect in an explicit manner, i.e. the smaller samples behave stiffer than larger samples of the same material. Consequently, such size effect has been successfully applied to the multiscale approach methods /8/.

MULTI-SCALE THEORETICAL AND NUMERICAL APPROACH VIA COSSERAT ISOTROPIC ELASTICITY

This section briefly describes the principle of Cosserat theory. Let us begin by establishing the coupled kinematical relations for the linear Cosserat-based media, /9/:

$$\bar{\varepsilon}^T = \nabla u - \bar{A}\,, \text{ where } \nabla u := (\nabla \otimes u)^T = u_{i,j}\hat{e}_i \otimes \hat{e}_j \text{ and } \bar{A} = -e_{ijk}\phi_k \hat{e}_i \otimes \hat{e}_j \tag{1a}$$

$$k = \nabla\phi\,, \text{ where } \nabla\phi := (\nabla\otimes\phi)^T = \phi_{i,j}\hat{e}_i\otimes\hat{e}_j \text{ for i,j = 1,2,3} \tag{1b}$$

$$u_{|\Gamma} = u_d\,, \text{ essential or Dirichlet displacement boundary conditions} \tag{1c}$$

where $u\in\mathbb{R}^3$, $\phi\in\mathbb{R}^3$, $\bar{A}\in\mathrm{SO}(3)\subset\mathbb{R}^3\times\mathbb{R}^3$, $e\in\mathbb{R}^{27}$ and $k\in\mathbb{R}^3\times\mathbb{R}^3$ are the displacement vector, micro-rotation vector, dual tensor of the micro-rotation vector, third-rank permutation tensor or Levi-Civita tensor and curvature tensor or so-called wryness tensor, respectively. We collect the balance equations excluding the body force and body moment vectors under strong form (see /8, 9, 10/ to get more details all about the variational approach and the virtual work principle of the linear isotropic Cosserat and micro-stretch theory), the constitutive laws for the isotropic Cosserat elasticity models and essential or Dirichlet boundary conditions including the relation between the micro-dilatation vector and its dual tensor:

$$\mathrm{Div}\,\sigma = f\,, \tag{2a}$$

$$-\mathrm{Div}\,m = 4\mu_c\cdot\mathrm{axl}(\mathrm{skew}\,\bar{\varepsilon})\,, \tag{2b}$$

$$\sigma = 2\mu\cdot\mathrm{sym}\,\bar{\varepsilon} + 2\mu_c\cdot\mathrm{skew}\,\bar{\varepsilon} + \lambda\cdot\mathrm{tr}\left[\bar{\varepsilon}\right]\cdot 1\!\!1 \text{ or } \sigma = 2\mu\cdot\mathrm{dev\,sym}\,\bar{\varepsilon} + 2\mu_c\cdot\mathrm{skew}\,\bar{\varepsilon} + K\cdot\mathrm{tr}\left[\bar{\varepsilon}\right]\cdot 1\!\!1$$

$$m = (\gamma+\beta)\,\mathrm{dev\,sym}\,\nabla\phi + (\gamma-\beta)\,\mathrm{skew}\,\nabla\phi + \frac{3\alpha+(\gamma+\beta)}{2}\mathrm{tr}\left[\nabla\phi\right]1\!\!1 \tag{2c}$$

$$\phi = \mathrm{axl}\,\bar{A} = -e_{ijk}A_{jk}\hat{e}_i \text{ for i,j = 1,2,3 and } u_{|\Gamma} = u_{\mathrm{d}}$$

where $\sigma\in\mathbb{R}^3\times\mathbb{R}^3$, $m\in\mathbb{R}^3\times\mathbb{R}^3$, $e\in\mathbb{R}^{27}$, $1\!\!1 = \delta_{ij}\hat{e}_i\otimes\hat{e}_j \in \mathrm{ISO}(3)\subset\mathbb{R}^3\times\mathbb{R}^3$, $\lambda = \dfrac{\nu E}{(1+\nu)(1-2\nu)}$, $\mu = G = \dfrac{E}{2(1+\nu)}$, and $K = \dfrac{3\lambda+2\mu}{3} = \dfrac{E}{3(1-2\nu)}$ are non-symmetric stress tensor, non-symmetric couple stress or stress moment tensor, third-rank Levi-Civita tensor and second-rank isotropic identity tensor, first and second Lamé's coefficients and bulk modulus, respectively. Let us provide the recently scrutinized curvature energy densities. These cases are well investigated by first author and Neff /11, 12, 13/ and it is numerically studied in /8, 14, 9/ by the first and third authors:

- Case1, Point-wise case /15/: This case corresponds to $\alpha = 0$, $\beta = 0$ and $\gamma = \mu L_c^2$

$$W_{\mathrm{curv}}(k) := \frac{\mu L_c^2}{2}k : k = \frac{\mu L_c^2}{2}\left\|k\right\|^2 \tag{3}$$

– Case1-1, Deviatoric point-wise case /16/: This case corresponds to $\alpha = -\dfrac{\mu L_c^2}{3}$, $\beta = 0$ and $\gamma = \mu L_c^2$

$$W_{\mathrm{curv}}(k) := \frac{\mu L_c^2}{2}\mathrm{dev}\,k : \mathrm{dev}\,k = \frac{\mu L_c^2}{2}\left\|\mathrm{dev}\,k\right\|^2 = \frac{\mu L_c^2}{2}\left(\left\|k\right\|^2 - \frac{1}{3}\mathrm{tr}^2\left[k\right]\right) \tag{4}$$

- Case2, Symmetric case /17, 18, 19, 20/: This case corresponds to $\alpha = 0$ and $\beta = \gamma = \dfrac{\mu L_c^2}{2}$

$$W_{\mathrm{curv}}(k) := \frac{\mu L_c^2}{2}\mathrm{sym}\,k : \mathrm{sym}\,k = \frac{\mu L_c^2}{2}\left\|\mathrm{sym}\,k\right\|^2 = \frac{\mu L_c^2}{2}\left(\frac{1}{2}\left\|k\right\|^2 + \frac{1}{2}\mathrm{tr}\left[k^2\right]\right) \tag{5}$$

- Case3, Conformal case /12, 8, 21, 22/: This case corresponds to $\alpha = -\dfrac{\mu L_c^2}{3}$ and $\beta = \gamma = \dfrac{\mu L_c^2}{2}$

$$W_{\text{curv}}(k) := \frac{\mu L_c^2}{2} \operatorname{dev}\operatorname{sym} k : \operatorname{dev}\operatorname{sym} k = \frac{\mu L_c^2}{2} \| \operatorname{dev}\operatorname{sym} k \|^2 = \frac{\mu L_c^2}{2} \left(\frac{1}{2} \| k \|^2 + \frac{1}{2} \operatorname{tr}\left[k^2 \right] - \frac{1}{3} \operatorname{tr}^2 \left[k \right] \right) \tag{6}$$

- Case4, Symmetric case with non-negative α, /9/: This case corresponds to $\alpha = \beta = \gamma$ and $\gamma = \mu L_c^2$

$$W_{\text{curv}}(k) := \frac{\mu L_c^2}{2} \left(k : k + k^T : k + \operatorname{tr}\left[k \right]^2 \right) = \frac{\mu L_c^2}{2} \left(\| k \|^2 + \operatorname{tr}\left[k^2 \right] + \operatorname{tr}^2 \left[k \right] \right). \tag{7}$$

In the present paper, we focus on the conformal case, i.e. Case 3 due to the fact that this case can provide the most stable parameters, /13/. Furthermore, this case is capable of describing the heterogeneous microstructures (see /12/ for more details). That is why we utilize the aforementioned case in modelling of the cement mortar behaviour at micro-structure in which the sand grains and cement matrix constitute a non-homogeneous mixture.

This characteristic length scale L_c, could be indirectly considered and interpreted as a dimension of *RVE* (Representative Volume Elementary) in the heterogeneous media. Let us now concentrate on the numerical torque experiments of our selected mortar specimen: consider a rectangular cement mortar bar (160×40×40 mm) subjected to a very small torsion angle (3°) at the end and fixed at the bottom.

The 3D-FEM computation is performed via the coupled system of Partial Differential Equations (PDEs) due to the coupled kinematic relation Eqs. (1a) and (1b). The outcomes of the rectangular Cosserat bar and the mechanical properties are plotted and indicated in a semi-logarithmic diagram (Fig. 1) where the stiffness of the material does not change until $L_c / L_{RVE} < 1$ corresponding to macrozone I. So far, we define the size of specimen RVE. Afterwards, the size effect starts to appear when $L_c > L_{RVE}$ corresponding to micro-zone II. The size of specimen on this state is $\text{RVE}^{\#}$. Finally, the increasing stiffness is bounded at $L_c \gg L_{RVE}$. That zone called nano-zone III would represent the smallest size specimen, RVE^0 still having a physical meaning.

Generally, L_c over the characteristic length L_{RVE} presents the material by itself as a whole and then the stiffness and the strength of the material will not be changed whatever the specimen size unless the size is greater or equal to RVE size. Consequently, the response from RVE is obviously a homogenized or an averaged value in the Cauchy's media. This indicates that our mortar $\text{RVE}^{\#}$ should be smaller than classical RVE. We can consider that $\text{RVE}^{\#}$ still contains a heterogeneous feature, i.e. cement paste and sand. However, it should be very small and it can be considered in zone III because it even involves even the chemical compositions of mortar. This does not make sense for the scale in which we concentrate on (Fig. 1).

BRIEF REVIEW ON THE EXPERIMENTAL STUDIES

Materials and testing methods

In this section, the experimental procedure of self-desiccation shrinkage and dynamic Young's modulus determination for our chosen mortar and their corresponding results are presented. The water-to-cement ratio (*W/C*) is equal to 0.3 throughout the paper and the aggregate-to-cement ratio (*A/C*) is equal to one.

The self-shrinkage test and dynamic Young's modulus measurements are performed in laboratory during the first 72 h of hydration. The measurement of the self-shrinkage is based on the principle of the hydrostatic weighing. The sample cast in a latex membrane, is placed on a nacelle and immersed in a thermostatted bath. The nacelle is afterwards suspended on the hook of a balance connected to a data logging system, which records the evolution of the apparent density of the specimen. It is well worth emphasizing that this volume reduction, or chemical shrinkage, begins immediately after mixing of water and cement and the rate is greatest during the first hours and days /24/. The magnitude of chemical shrinkage can be estimated using the molecular weight and densities of the compounds as they change from the basic to reaction products /25; 26/. Justnes et al. showed that the bleeding of the specimen could be an important cause of over-estimation of the early-age deformations /25/. In order to eliminate these artefacts, a waterproof motorized experimental device, allowing to put the specimen in continuous rotation, is developed herein, /27/. More details on the measuring technique can be found in /27/. The dynamic Young's modulus are determined on 160×40×40 mm rectangular bar via pulse excitation with a Grindosonic device. Each test is repeated three times and the extracted outcomes are used to calculate a mean value for the dynamic Young's modulus.

In order to investigate the early-age microstructure of the interfacial zone between cement paste and aggregates, Portland cement mortars are prepared with the siliceous sand as aggregates. As indicated previously, the aggregate-to-cement ratio is equal to one. The samples are observed by means of the Scanning Electronic Microscopy (SEM) technique. To achieve the SEM technique, all specimens are taken and wrapped in a polyethylene film and they are kept at 20 ± 2°C. They are then immersed in methanol to stop hydration, dried in a 40°C-oven during 4 hours and impregnated with a very fluid epoxy resin under vacuum, in order to fill the porosity. After a curing time of 14 hours in epoxy resin, the samples are polished with silicon carbide (of variable size up to 0.25 μm). Finally, they are covered with a 200-Å layer of palladium gold before introducing into the SEM chamber.

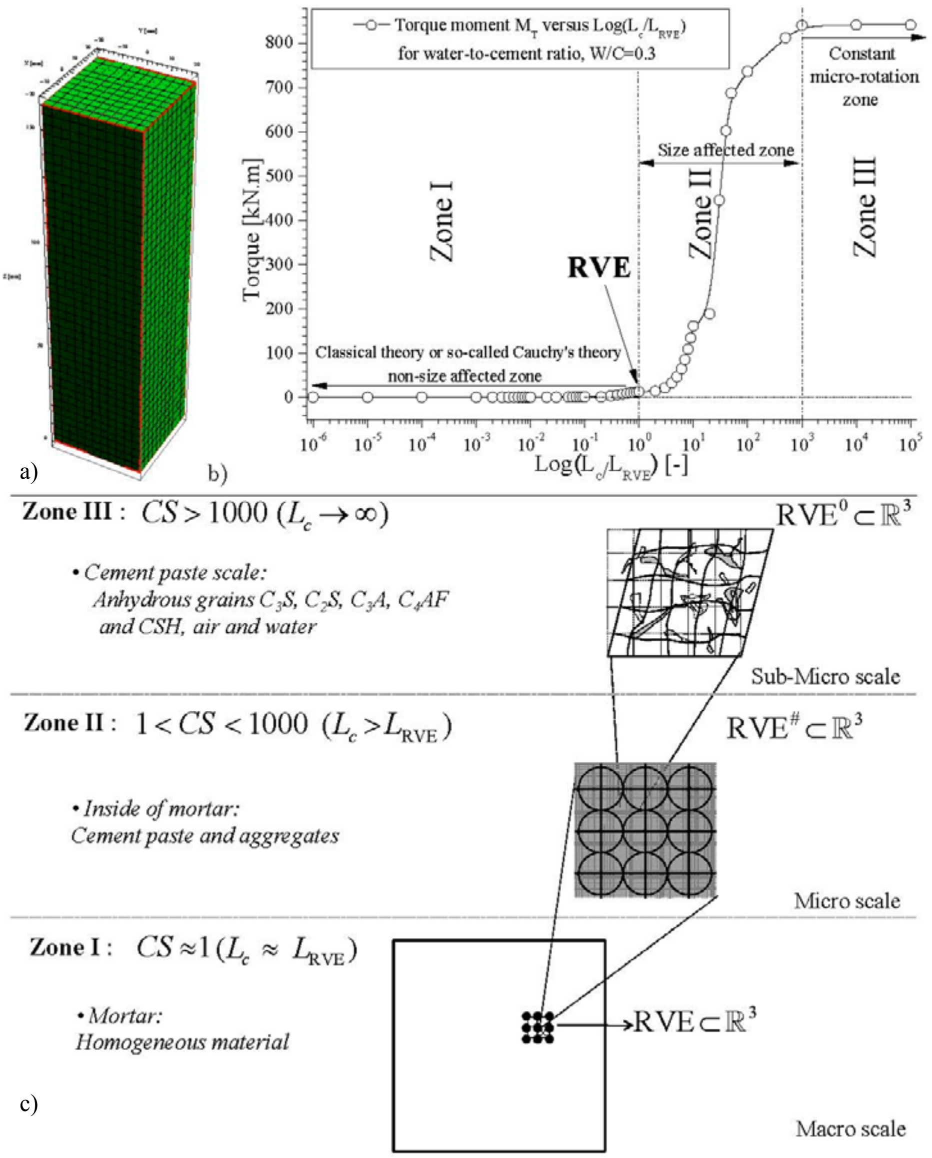

Figure 1. Relevant size effect with respect to Log(CS) or Log(L_c/L_{RVE}) via 3D-FEM numerical experiments of a rectangular Cosserat bar including 1.2 Mi DOFs, a) Geometrical configuration of our chosen rectangular Cosserat bar (160×40×40 mm), b) Semi-logarithmic diagram of torque moment versus Log(CS) or Log(L_c/L_{RVE}) for conformal case, i.e. $\alpha = -\dfrac{\mu L_c^2}{3}$, $\beta = \gamma = \dfrac{\mu L_c^2}{3}$ and $\mu_c = \mu = \dfrac{E}{3(1-2\nu)}$, c) Size effect phenomenon: numerical results of the increasing stiffness of the cement mortar bar subjected to the torque on the left hand side and its relevant multi-scale approach.

Slika 1. Relevantni uticaj dimenzija s obzirom na Log(CS) ili Log(L_c/L_{RVE}) preko 3D-FEM numeričkih eksperimenata pravougaone Kosera epruvete sa 1,2 mil. DOF, a) geometrija date pravougaone Kosera epruvete (160×40×40 mm), b) polu-logaritamski dijagram momenta sile u funkciji Log(CS) ili Log(L_c/L_{RVE}) za konformni slučaj, tj. $\alpha = -\dfrac{\mu L_c^2}{3}$, $\beta = \gamma = \dfrac{\mu L_c^2}{3}$ i $\mu_c = \mu = \dfrac{E}{3(1-2\nu)}$, c) fenomen uticaja dimenzija: numerički rezultati rasta krutosti epruvete od cementnog maltera, koja je podvrgnuta momentu sile sa leve strane i relevantni multiskalarni pristup.

Table 1. Size-independent and dependent mechanical properties of chosen cement-based mortar applied to the Cosserat conformal curvature energy assumption (Case 3) involving the rectangular Cosserat bar for extracting relevant so-called Cosserat size effect number CS = L_c/L_{RVE} corresponding to the microstructure.

Tabela 1. Dimenziono nezavisne i zavisne mehaničke osobine datog cementnog maltera primenjene u Kosera konformne krivolinijske energijske pretpostavke (Slučaj 3) sa pravougaonom Kosera epruvetom za određivanje relevantnog takozvanog broja Kosera dimenzionog uticaja CS = L_c/L_{RVE} koji se odnosi na mikrostrukturu.

Material constants name	Material constants values
Water-to-cement ratio, W/C [–]	0.3
Modulus of elasticity, E [N/mm^2]	30×10^3
Poisson's ratio, ν [–]	0.28
Cosserat couple modulus, μ_c [N/mm^2]	$\mu_c = \mu = E/2(1+\nu)$
Characteristic length scale, L_c [mm]	$0 \le L_c \le 10^5$
RVE size, L_{RVE} [mm]	100 (see /23/ for more details)
Cosserat Size effect number, CS = L_c/L_{RVE} [–]	$10^{-5} \le CS \le 10^5$

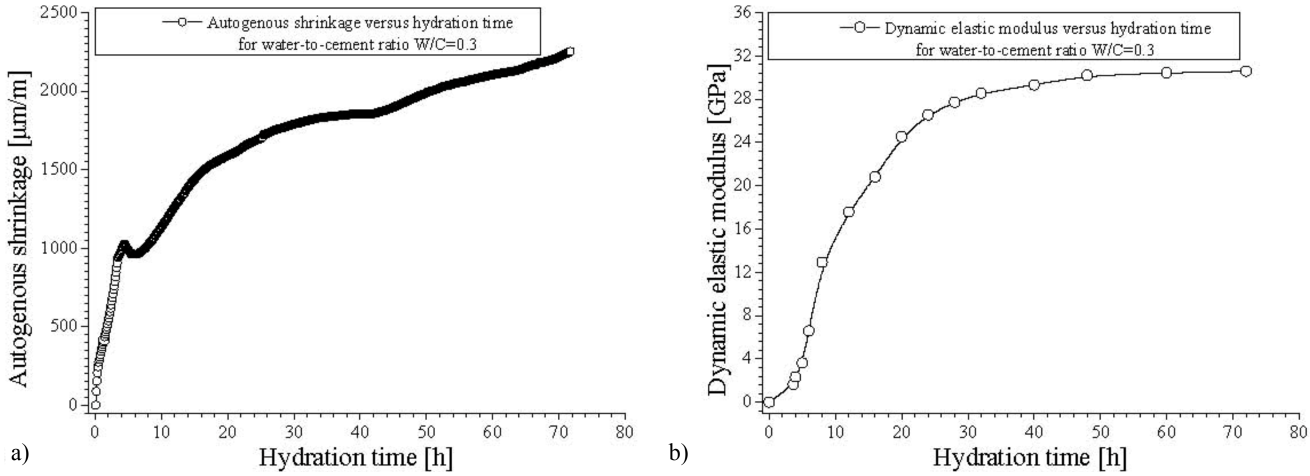

Figure 2. Properties of chosen cement paste with $W/C = 0.30$ and $A/C = 1$, a) Volumetric autogenous shrinkage vs. hydration time, b) Dynamic Young's modulus vs. hydration time.

Slika 2. Osobine date cementne paste sa $W/C = 0.30$ i $A/C = 1$, a) zapreminsko autogeno skupljanje u funkciji vremena hidratacije, b) dinamički Jungov modul u funkciji vremena hidratacije.

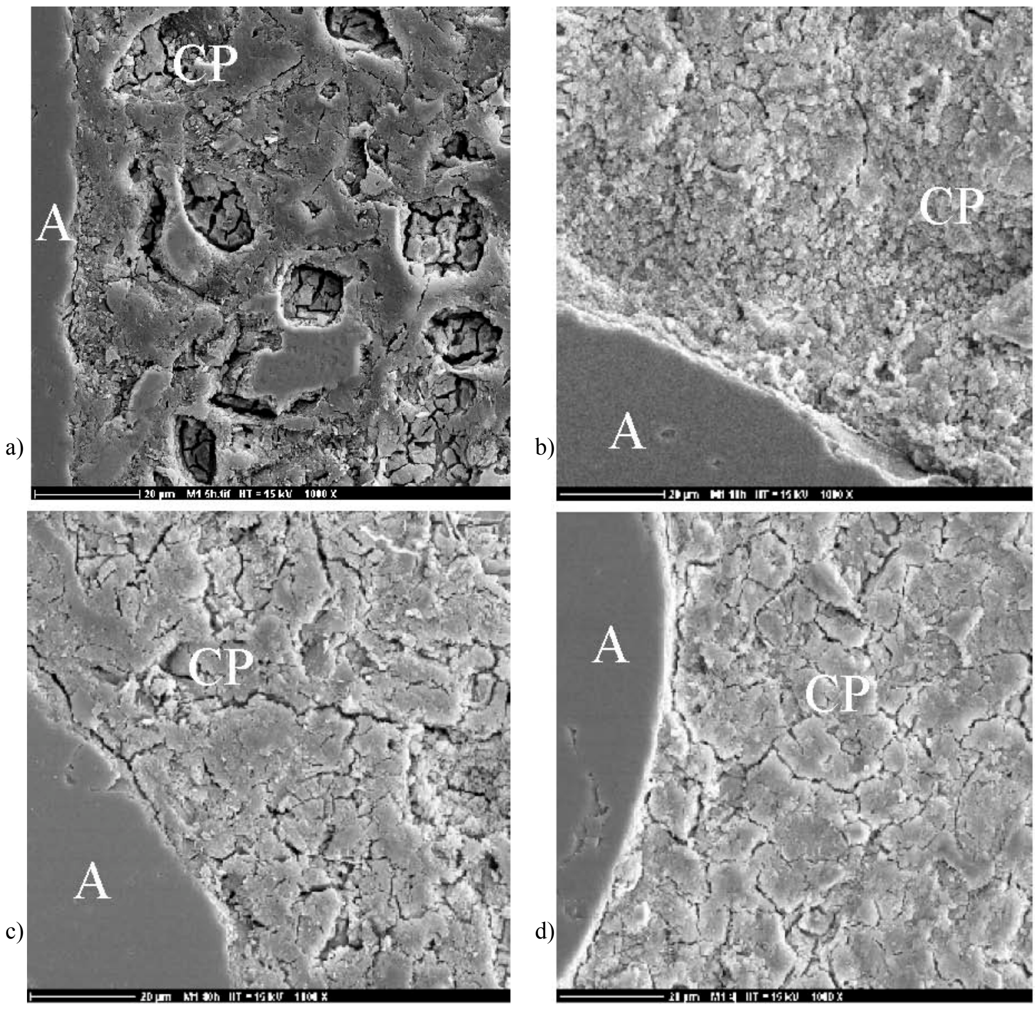

Figure 3. SEM images of our chosen mortar with $W/C = 0.3$ and $A/C = 1$ (A and CP stand for siliceous sand and cement paste) at: a) 5 h, b) 10 h, c) 48 h, d) 96 h.

Slika 3. SEM snimci datog maltera sa $W/C = 0.3$ i $A/C = 1$ (A i CP označavaju silikatni pesak i cementna pasta) na: a) 5 č, b) 10 č, c) 48 č, d) 96 č.

Test results

The experimental results are displayed in Fig. 3 and Fig. 2: We can readily see a very rapid evolution of shrinkage phenomena at very early age before 48 hours after mixing and then an asymptotic self-desiccation behaviour is seen (see /28, 27/ to get more details pertaining to the experimental setup and procedures).

During the self-desiccation process, the microstructure of samples and particularly the cement paste aggregate interface is observed using SEM images at 5 h, 10 h, 18 h and 48 h (Fig. 3).

The dynamic modulus of elasticity of mortar constantly grows at the early age (Fig. 2b) so that the matrix is no longer enough smooth or flexible to bear and withstand against the deformations induced by the self desiccation of the porous network. That would cause micro-cracking in cement paste and specially at the interface among the grains. It is necessary to emphasize that the micro-cracking issue at the early age and beyond is an important topic in the cement and concrete society. One can address some experimental investigations, e.g. Kim and Weiss /29/ (acoustic emission for micro-cracks detection), Neithalath et al. /30/, Puri and Weiss (assessment of localised damage) /31/, Hossain and Weiss (impact of the specimen geometry and boundary conditions) /32/, Soulioti et al. /33/ and some other relevant works /34, 35, 36/.

HYGRO-COSSERAT APPROACH FOR SELF-DESICCATION SHRINKAGE OF CEMENT MORTAR

After determining the changing scale parameter $L_c/L_{RVE} = 100$ corresponding to the micro-scale we would like to investigate the hygro-mechanical approach based on the Cosserat theory: it enables us to model the generating hygro-stresses due to autogenous shrinkage deformation in mortar during the hydration process, particularly at the micro-scale when the specimen is as small as RVE[#] according to our multi-scale consideration. To derive the constitutive laws for the considered hygro-micropolar problem, we put into practice the additive strain decomposition rule well-known as Duhamel-Neumann rule which is commonly applied into the infinitesimal deformations /37/ (see comment):

$$\overline{\varepsilon} := \overline{\varepsilon}^{\mathcal{M}} + \overline{\varepsilon}^{\mathcal{H}} \tag{8a}$$

$$\text{where } \overline{\varepsilon}^{T} = \nabla u - \overline{A} \quad \text{and} \quad \varepsilon^{\mathcal{H}} = \alpha^{\mathcal{H}} \cdot \Delta \mathrm{II} \cdot \mathrm{ll} \tag{8b}$$

$\alpha^{\mathcal{H}}$ is the hygric coefficient and $\Delta\mathrm{II} \in [0, 1] \subset \mathbb{R}^+$ is the relative humidity variation between initial and current situation. In the above Eq. (8a), $\varepsilon^{\mathcal{M}} \in \mathbb{R}^3 \times \mathbb{R}^3$ and $\varepsilon^{\mathcal{H}} \in \mathrm{ISO}(3) \subset \mathbb{R}^3 \times \mathbb{R}^3$ are the mechanical second-rank strain tensor and hygric-induced second-rank strain tensor which is mostly assumed as an isotropic tensor, respectively. The autogenous shrinkage $\varepsilon^{\mathcal{H}}$ at early age of the cement paste has been measured in laboratory to introduce in (8a) as well as the dynamic elasticity modulus in Fig. 2.

Comment: The additive strain measurement decomposition method is widely utilised in calculating the deformations of the infinitesimal coupled problems. The most complete strain measurement or finite deformation would be extracted via the multiplicative decomposition of deformation gradient tensor $F = \mathrm{ll} + \nabla u$:

$$F = F^{\mathcal{M}} F^{\mathcal{H}} \tag{9}$$

where, $F^{\mathcal{M}}$ and $F^{\mathcal{H}}$ are mechanical part of deformation gradient tensor $F \in \mathbb{R}^3 \times \mathbb{R}^3$ and its hygric counterpart, respectively. Some benchmark studies promising these kinds of strain measurements could be addressed in /38, 39/.

Consider a cement paste cube representing RVE[#], which includes several spherical sand grains (1 up to 10) for our hygro-mechanical stress computations. According to the extracted outcomes, first at all, we observe the hygro-mechanical stresses whose magnitude drastically increased during the first hours of hydration and then they turn out to be nearly stable. Moreover, we find out that one-grain-cube creates very high stress (45 MPa) merely around the grain at 48 h while ten-grain-cube generates less stress (15 MPa). In the meanwhile, the stress is smoothly distributed among the grains providing one micro-crack network at 48 h after mixing up stage. These numerical results can explain and confirm the presence of micro-cracks around the sand grains and these networks are readily captured via SEM observations (see Figs. 3, 4 and 5).

CONCLUSION

In this paper, a novel multi-scale theoretical and numerical approach is investigated for capturing the micro-crack initiation next to the sand grains due to autogenous shrinkage in cement based mortar materials. To achieve it, the changing scale ratio, i.e. $L_c = L_{RVE}$ is proposed based on the size effect phenomenon of linear isotropic Cosserat elasticity. The last parameter relating to the RVE of the considered cement mortar material allows us to reduce the size of specimen until quite small size in which the micro-crack initiation can be seen. Nevertheless, it is not large enough to capture the chemical components. Using the additive strain decomposition rule, the hygro-mechanical stresses in the mortar could be numerically computed at early age of hydration. It is well worth noting that autogenous shrinkage of the mortar is obtained by the experiments as well as the dynamic Young's modulus which is used in the numerical computation. According to the numerical results, it is found that the number of inclusions influences the magnitude of hygro-mechanical stresses around the sand grains, the higher number of inclusions inducing the greater stresses. This fact can be easily distinguished and substantiated by the SEM observations at this scale.

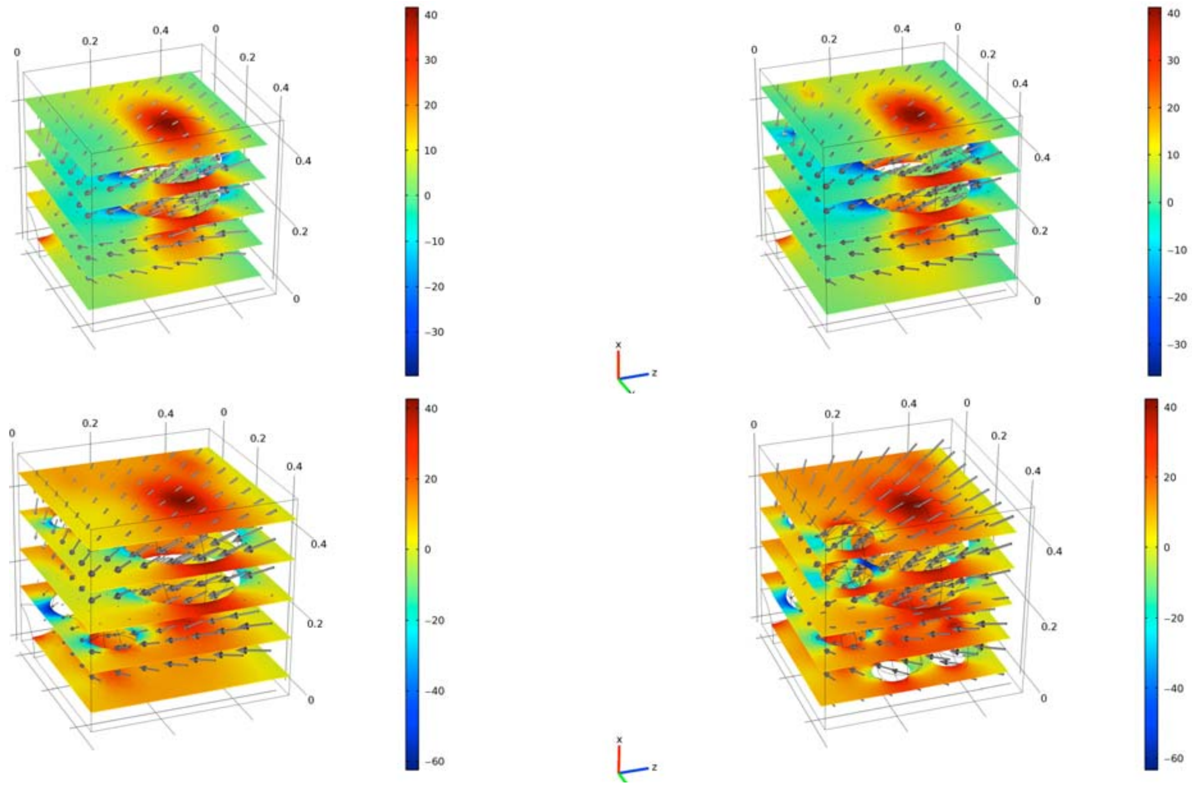

Figure 4. Hygro-mechanical stress development in function of the hydration time for $RVE^{\#} \subset \mathbb{R}^3$ cube at 48 hours after mixing,
a) Case study I, b) Case study II, c) Case study III and d) Case study IV.
Slika 4. Razvoj higro-mehaničkog napona u funkciji vremena hidratacije za $RVE^{\#} \subset \mathbb{R}^3$ kocku 48 č. nakon mešanja,
a) slučaj I, b) slučaj II, c) slučaj III i d) slučaj IV.

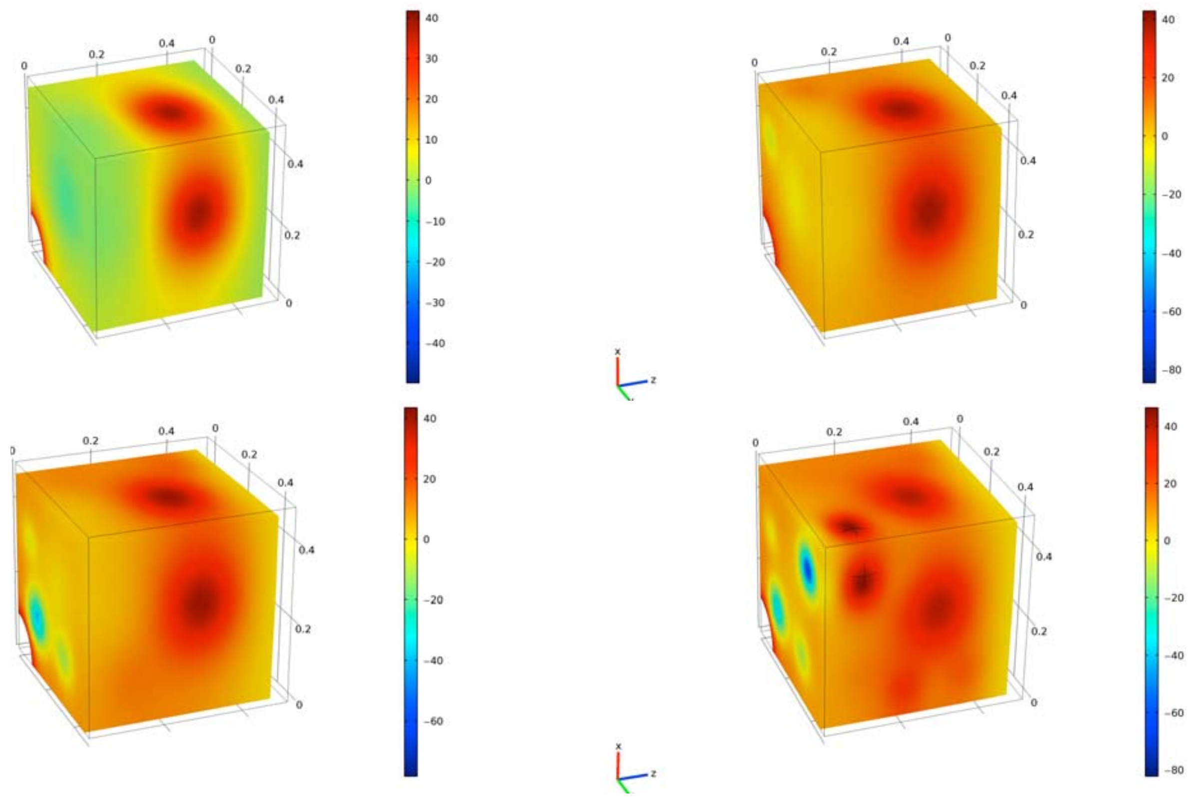

Figure 4. Hygro-mechanical stress of $RVE^{\#} \subset \mathbb{R}^3$ cube under deformed shape at 48 hours after mixing,
a) Case study I, b) Case study II, c) Case study III and d) Case study IV.
Slika 4. Higro-mehanički napon za $RVE^{\#} \subset \mathbb{R}^3$ kocku u deformisanom stanju 48 č. nakon mešanja,
a) slučaj I, b) slučaj II, c) slučaj III i d) slučaj IV.

REFERENCES

1. Cosserat, E., Cosserat, F., Théorie des corps déformables. Librairie Scientifique A. Hermann et Fils (engl. translation by D. Delphenich 2007, http://www.mathematik.tu-darmstadt.de/fbereiche/analysis/pde/staff/neff/patrizio/Cosserat.html), Paris, 1909.
2. Cosserat, E., Cosserat, F., Note sur la théorie de l'action euclidienne. P. Appell, editor, Traité de Mécanique Rationelle., volume III, pp.557-629. Gauthier-Villars, Paris, 1909.
3. Günther, W., *Zur statik und kinematik des cosseratschen kontinuums*, Abh. Braunschweig Wiss. Ges., 10 : 195-213, 1958.
4. Mindlin, R.D., Tiersten, H.F., *Effects of couple stresses in linear elasticity*, Arch. Rat. Mech. Anal., 11 : 415-447, 1962.
5. Eringen, A.C., Suhubi, E.S., *Nonlinear theory of simple micro-elastic solids*, Int. J. Eng. Sci., 2 : 189-203, 1964.
6. Eringen, A.C., Kafadar, C.B., Polar Field Theories. Ed. A.C Eringen, Continuum Physics, volume IV: Polar and Nonlocal Field Theories, pages 1-73. Academic Press, New York, 1976.
7. Eringen, A.C., Microcontinuum Field Theories, Springer, Heidelberg, 1999.
8. Jeong, J., Ramézani, H., Münch, I., Neff, P., *Simulation of linear isotropic Cosserat elasticity with conformally invariant curvature*, Z. Angew. Math. Mech., 89 (7) : 552-569, 2009.
9. Jeong, J., Ramézani, H., *Enhanced numerical study of infinitesimal non-linear Cosserat theory based on the grain size length scale assumption*, Computer Methods in Applied Mechanics and Engineering, In Press, Corrected Proof: 2010.
10. Neff, P., Jeong, J., Münch, I., Ramézani, H., *Mean field modeling of isotropic random Cauchy elasticity versus microstretch elasticity*, Z. Angew. Math. Phys., 60 (3) : 479-497, 2009.
11. Jeong, J., Neff, P., *Existence, uniqueness and stability in linear Cosserat elasticity for weakest curvature conditions*, Mathematics and Mechanics of Solids, 15 (1) : 78-95, 2010. First published on Sep. 17, 2008, doi:10.1177/1081286508093581.
12. Neff, P., Jeong, J., *A new paradigm: the linear isotropic Cosserat model with conformally invariant curvature energy*, Z. Angew. Math. Mech., 89 (2) : 107-122, 2009.
13. Neff, P., Jeong, J., Fischle, A., *Stable identification of linear isotropic Cosserat parameters: bounded stiffness in bending and torsion implies conformal invariance of curvature*, Acta Mechanica, 211 (3) : 237-249, May 2010.
14. Jeong, J., Ramézani, H., *Implementation of the finite isotropic linear Cosserat models based on the weak form*, Scientific committee of European Comsol Conference in Hannover-Germany, Ed. European Comsol Users Conference 2008, Nov. 2008.
15. Münch, I., Ein geometrisch und materiell nichtlineares Cosserat-Modell-Theorie, Numerik und Anwendungsmöglichkeiten, PhD thesis, University of Karlsruhe (TH), Oct. 2007.
16. Lakes, R.S., *On the torsional properties of single osteons*, J. Biomech., 25 : 1409-1410, 1995.
17. Zastrau, B., *Zur Berechnung orientierter Kontinua - Entwicklung einer Direktorentheorie und Anwendung der Finiten Elemente*, Number 4/60 in Fortschrittberichte der VDI Zeitschriften, Verein Deutscher Ingenieure, VDI-Verlag GmbH, Düsseldorf, 1981.
18. Zastrau, B., Rothert, H., *Herleitung einer Direktortheorie für Kontinua mit lokalen Krümmungseigenschaften*, Z. Angew. Math. Mech., 61 : 567-581, 1981.
19. Borst, E. de, *Simulation of strain localisation: a reappraisal of the Cosserat continuum*, Eng. Comput., 8 (4) : 317-332, 1991.
20. Forest, S., Dendievel, R., Canova, G.R., *Estimating the overall properties of heterogeneous Cosserat materials*, Modelling Simul. Mater. Sci. Eng., 7 : 829-840, 1999.
21. Neff, P., Jeong, J., Ramézani, H., *Subgrid interaction and micro-randomness - novel invariance requirements in infinitesimal gradient elasticity*, International Journal of Solids and Structures, 46 (25-26) : 4261-4276, 2009.
22. Neff, P., Jeong, J., Münch, I., Ramézani, H., *Linear Cosserat Elasticity, Conformal Curvature and Bounded Stiffness*, G.A. Maugin, V.A. Metrikine, Eds., Mechanics of Generalized Continua, One hundred years after the Cosserats, volume 21 of Advances in Mechanics and Mathematics, pp.55-63. Springer, Berlin, 2010.
23. Pichler, C., Lackner, R., Mang, H.A., *A multiscale micromechanics model for the autogenous-shrinkage deformation of early-age cement-based materials*, Engineering Fracture Mechanics, 74 (1-2) : 34-58, 2007. Fracture of Concrete Materials and Structures.
24. Holt, E., *Contribution of mixture design to chemical and autogenous shrinkage of concrete at early ages*, Cement and Concrete Research, 35 (3) : 464-472, 2005.
25. Justnes, H., Sellevold, E.J., Reyniers, B., Van Loo, D., Van Gemert, A., Verboven, F., Van Gemert, D., *The influence of cement characteristics on chemical shrinkage*, Londres: E FN Spon, Ed., Proc. of Intern. Workshop on Autogenous Shrinkage of Concrete Autoshrink 98, pp.71-80, 1998. Hiroshima (Japan).
26. Holt, E., Early age autogenous shrinkage of concrete, PhD thesis, University of Washington, Seattle, 2001.
27. Bouasker, M., Mounanga, P., Khelidj, A., Cou, R., *Free autogenous strain of early age cement paste: Metrological development and critical analysis*, Advances in Cement Research, 20 (2) : 75-84, 2008.
28. Bouasker, M., Étude numérique et expérimentale du retrait endogène au très jeune âge des pâtes de ciment avec et sans inclusions, PhD thesis, University of Nantes, November 2007.
29. Kim, B., J. Weiss, *Using acoustic emission to quantify damage in restrained fiber-reinforced cement mortars*, Cement and Concrete Research, 33 (2) : 207-214, 2003.
30. Neithalath, N., Weiss, J., Olek, J., *Acoustic performance and damping behavior of cellulose-cement composites*, Cement and Concrete Composites, 26 (4) : 359-370, 2004.
31. Puri, S., Weiss, J., *Assessment of localized damage in concrete under compression using acoustic emission*, Journal of Materials in Civil Engineering, 18 (3) : 325-333, 2006.
32. Hossain, A.B., Weiss, J., *The role of specimen geometry and boundary conditions on stress development and cracking in the restrained ring test*, Cement and Concrete Research, 36 (1) : 189-199, 2006.
33. Soulioti, D., Barkoula, N.M., Paipetis, A., Matikas, T.E., Shiotani, T., Aggelis, D.G., *Acoustic emission behavior of steel fibre reinforced concrete under bending*, Construction and Building Materials, 23 (12) : 3532-3536, 2009.
34. Lura, P., Couch, J., Mejlhede Jensen, O., Weiss, J., *Early-age acoustic emission measurements in hydrating cement paste: Evidence for cavitation during solidification due to self-desiccation*, Cement and Concrete Research, 39 (10) : 861-867, 2009.
35. Rougelot, T., Skoczylas, F., Burlion, N., *Water desorption and shrinkage in mortars and cement pastes: Experimental study and poromechanical model*, Cement and Concrete Research, 39 (1) : 36-44, 2009.
36. Grassl, P., Wong, H.S., Buenfeld, N.R., *Influence of aggregate size and volume fraction on shrinkage induced micro-cracking of concrete and mortar*, Cement and Concrete Research, 40 (1) : 85-93, 2010.
37. Saad, M.H., Elasticity: theory, application and numerics, Elsevier Butterworth-Heinemann, 2005.
38. Lubarda, V.A., *Constitutive theories based on the multiplicative decomposition of deformation gradient: Thermoelasticity, elastoplasticity, and biomechanics*, Applied Mechanics Reviews, 57 (2) : 95-108, 2004.
39. Muñoz, J.J., Barrett, K., Miodownik, M., *A deformation gradient decomposition method for the analysis of the mechanics of morphogenesis*, Journal of Biomechanics, 40(6):1372-1380, 2007.